Robotic Positioning for Quality Assurance of Feature-Sparse Components using a Depth-Sensing Camera

Adam Gilmour, William Jackson, Dayi Zhang, *Member, IEEE*, Gordon Dobie, Charles N. MacLeod, Benjamin Karkera, Thomas Barber

Abstract— **In this paper, a novel method for crawler positioning is presented utilizing an onboard depth-sensing camera which can operate in semi-structured, self-similar environments, using only measurements of the sample under inspection to navigate. Non-destructive evaluation at manufacture is a vital aspect of assuring the fitness for purpose of high-value marine assets, moreover, it is almost always a regulatory requirement to ensure build quality standards have been met. Traditionally these inspections were deployed manually by a trained operator in a laborious and time-consuming manner. More recently, robotic crawler-based solutions have become available on the marketplace, however, these solutions are limited in their capabilities and still require significant manual intervention and set-up for each application. Additionally, GPS or prior knowledge of their surroundings which are critical to their operation are often unavailable in an active work environment. An autonomous, self-localizing system would provide significant benefits in these situations, but certain challenges arise from limited situational awareness and poor positional accuracy. The accuracy and robustness of the novel method were assessed and experimentally validated through ground truth readings from a Vicon motion capture system. The localization algorithm's ability to function on different materials and under various lighting conditions was also explored. Using the example of the receipt inspection of steel plate under 240 lux lighting, the system proved capable of positioning the crawler at the desired position within 5.7mm.**

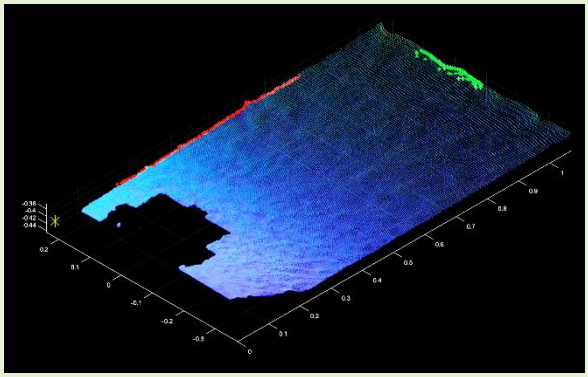

***Index Terms*— NDE, Edge Detection, Point Cloud, Robotic Crawler, Robot Localization**

I. Introduction

NON-DESTRUCTIVE EVALUATION (NDE) is a method of assessing both the internal and external integrity of engineering components without the need to physically alter the material. The use of NDE techniques is prevalent in the manufacturing sector as a means of establishing a baseline standard of quality for final products.

This is of particular importance within UK defense for the manufacture of marine assets where reassurance of a structure's condition is critical in prolonging their working life and in assuring the safety of personnel aboard said assets [1].

In its current form, the hand acquisition of this data is time-consuming and laborious. To support NDE inspectors, the use of robotic crawlers can be implemented to aid in a number of aspects including providing access to unreachable or enclosed areas, assisting in probe alignment, decreasing the inspection time, and generally improving the health & safety aspects associated with conducting inspections [2]. These are often specialized robotic systems and are typically suited towards well-defined geometries [3] but are limited by a high degree of manual intervention, lack a general-purpose design, and implement unnecessary bulk data acquisition.

This is also reflected within commercial products such as the Scorpion 2 and Stingray [4], [5], which are limited to a single application, corrosion mapping, and are manually controlled maintaining the time investment of operators to carry out the inspection. Other products like the Navic, SAW Bug, and the Fast UT system [6]–[8] offer semi-autonomous positioning and alignment for the inspection of welds. Relying, however, on specific features e.g. the presence of a weld cap, to track the area of interest, limiting its scope.

A general-purpose solution implies that there is a wide range of operational working environments, hence requiring robust and accurate robot positioning, especially when considering autonomous inspection. The challenge of robot localization is well explored with ongoing research of techniques such as Simultaneous Localization and Mapping (SLAM) [9] and 3D Scan Matching [10]. Both are powerful tools achieving precise localization within a lab setting [11], [12], however, this does not always transpire into real-world accuracy. Within an industrial setting crawler positional errors have been observed to reach 0.38 m [13] and elements that can aid in performance

This work was supported by the Centre for Doctoral Training in Future Innovation in NDE (FIND-CDT) and BAE Systems under Grant EP/S023275/1.

Adam Gilmour, William Jackson, Dayi Zhang, Gordon Dobie, and Charles N. MacLeod are with the Centre for Ultrasonic Engineering (CUE), University of Strathclyde, Glasgow, G1 1XW, U.K. (e-mail: adam.gilmour@strath.ac.uk). Benjamin Karkera and Thomas Barber are with BAE Systems, Barrow-in-Furness, LA14 1AF, U.K.

such as GPS or prior knowledge of surroundings are often unavailable. In addition, industrial settings tend to be active working environments with various pieces of machinery and personnel operating within its confines, hampering the performance of both SLAM and Scan Matching. This active environment provides a challenge where crawler localization is limited to features associated to the component or structure being investigated.

Novel techniques of localized crawler positioning are available with the challenge simplified through priori knowledge of the industrial asset [14], [15], achieving accuracies of 5-10 mm from the desired position. These setups also benefit from using small on-board sensors which offer flexible functionality at a low cost when compared to high accuracy, external alternatives such as photogrammetry [16] and laser based systems [17].

An issue arises within UK defense where prior knowledge of both the setting and parts under inspection are restricted for confidentiality. Thus, requiring a complete standalone system capable of navigation and strong positional awareness from a zero-assumption starting position. An example of Occupancy Grid Mapping was utilized for a similar application where guided waves were propagated through steel plate using Electromagnetic Acoustic Transducers (EMATs) [18]. Despite the success of this method the type of generated wave depends upon the thickness of the propagating material. For applications such as the receipt inspection of steel plate, a requirement in the early stages of maritime manufacture, which is performed on a range of plates varying in size and thickness. Hence, an array of EMATs would be required to cover the spectrum of geometry and lengthy preparation would be required by the inspector.

The receipt inspection of steel plate is governed by defense and British standards which detail a specific area of coverage requiring manual measurements taken with an ultrasonic thickness probe. The inspection is not a full volumetric scan of the material, but rather, only 10% of the plates surface is investigated. The raw material is measured manually to find the gauge thickness of the plate and to search for indications of laminations and inclusions which can form during fabrication of the plate [19]. The pattern is defined as a grid of linear scans separated by a ratio of the plate's width, similar to Fig. 1. The main disadvantage with this process is the time investment made by an inspector to prepare the plate and in taking manual readings across the span of their large area. Resulting in an inefficient use of a skilled operator's time. The implementation of a robotic system would also increase the repeatability of the measurement acquisition, ensuring a consistent path is followed for every inspection without the risk of dropping quality due to operator fatigue. This application is of particular interest as it parallels situations that can be recognized in many other settings. The surface is planar and semi-structured with the added complexity of showing self-similarity when focusing solely on the plate.

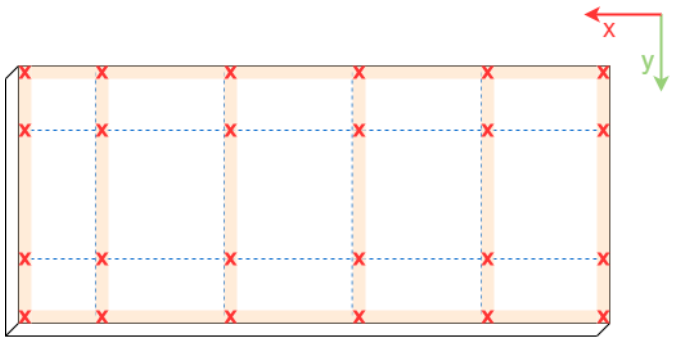

Fig. 1. Scan Pattern required for the receipt inspection. The red crosses indicate points for individual gauge thickness measurement and the orange shaded regions represent scan paths for laminations and inclusions.

This paper therefore presents a novel method of autonomous crawler localization for such environments, implementing an on-board RGB-Depth camera to monitor the oncoming geometry of the plate as a crawler crosses it surface. Through post-processing the crawler's position relative to the edge of it's traversable universe can be monitored, requiring minimal prior knowledge of the raw material to do so. The goal being to maintain a 200 mm distance from the crawler's center to the plates edge. A performance study of the Intel RealSense D435i RGBD camera is also conducted, specifically, its ability to guide a 4-wheeled differential drive crawler during the receipt inspection described previously. Practical considerations are taken into account including the light level of the environment as industrial storage often takes the form of large open ended hangers. Resulting in a light gradient from the exposed entrance to the sheltered rear end of the building which can affect measurements taken by the camera [13], [20], [21]. The plate investigated for the receipt inspection is structural steel, however, the camera's ability to operate with different materials is explored to better understand the extent of its capabilities and to gain an insight into other potential applications.

In section II the crawler hardware is listed along with information regarding the experimental setup and procedure for testing. Section III introduces the novel method of crawler localization and details the process of capturing raw point cloud data to monitor the crawler position while running. Section IV then explains the results and ultimately the performance of the system for both static and dynamic testing before conclusions and future work are drawn in section V.

The contributions of this paper are:

- The post-processing of RGBD camera data to extract the edges of plate using depth data.
- Development of a novel robotic localization technique capable of autonomous navigation using only generic features of the inspection material.
- Evaluation of post processing and localization algorithms under different working conditions.

II. Setup

A. Equipment Configuration

The D435i is a stereo vision camera and was selected due to its form factor, global shutter for simultaneous exposure between all pixels, wide field of view to capture maximum

environmental information, high frame rate, and low cost, Table 1 [22]. Studies have also been caried out assessing the the noise related to the camera and the distance dependant depth error which was limited to ≤ 35 mm up to a range of 2.0 m [23]. The D435i itself and the wider Realsense series of Intel cameras are also tried and tested in the field of robotic navigation. They have been used in agriculture based object detection and path planning [13], indoor visual SLAM [24], [25], and in-field robotics [20]. The camera compliments two wheel encoders aboard a 4-wheeled differential drive crawler, Fig. 2. The pair of wheel encoders provide information regarding the crawler's displacement but are primarily responsible for regulating the wheel speeds. The crawler origin is defined as the mid-point of the center line between the encoder pair which is the point used for positional tracking throughout the research. The D435i is fixed above the crawler and pitched down to focus on a region $0.1 < x < 1.8$ m in front of the crawler. This region is selected to reflect the size of sample used for testing, a 2 x 1 m carbon steel plate which was the maximum size possible within the laboratory. It is aligned so that camera's y-axis is parallel to the crawler's y-axis while variations in the camera's pitch are accounted for through an automated correction procedure carried out for every reading. For the investigation of other surfaces the materials were sized to cover the capture region. A full list of experimental hardware is displayed in Table 2.

Table 1
Intel RealSense D435i Specification

Sensor Technology	Global Shutter
Depth FoV (H x V)	87° x 58°
Depth resolution	Up to 1280 x 720
Depth Accuracy	< 2 % at 2 m
Depth Frame Rate	Up to 90 fps

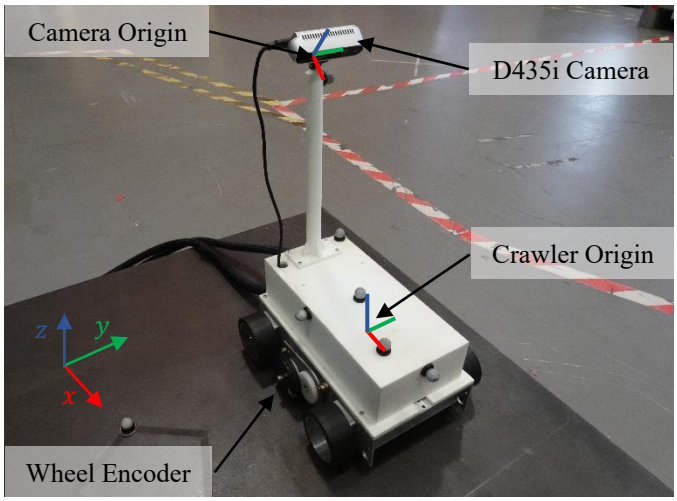

Fig. 2. Crawler configuration, a 4-wheel differential drive crawler is combined with twin wheel encoders and Intel RealSense D435i depth camera.

Table 2
Hardware used during study.

Experimental Hardware
Intel RealSense D435i Depth Sensing Camera
Kubler Rotary wheel Encoder (x2) (8.3700.1322.1024)
Eddyfi Scorpion 2 Crawler Base
Standard Carbon Steel Plate (2 x 1 m)
Standard Polished Aluminum Plate (2 x 1 m)
High Grade White Paper (2 x 1 m)

B. Experimental Procedure

Two types of testing were undertaken during the assessment of the system. Static tests were carried out to understand how reliably the edge detection performed across a number of measurements whilst the crawler remained motionless. Dynamic tests were then conducted where the localization algorithm was engaged allowing the crawler to traverse the plate.

For both experiments point cloud images were captured and processed identically as described in section III. For static testing the crawler was placed 200 mm from the parallel edge and 1400 mm from the perpendicular edge as seen in Fig. 3. MATLAB was used to capture individual depth frames from the camera and process the point cloud to produce a positional estimate for the crawler relative to the plates edge. Translational and rotational information of both the plate and crawler were also recorded simultaneously within a global reference frame using a Vicon motion capture system. This method is used due the high level of accuracy achieved with a fully calibrated rig, with system errors noted at below 1 mm [16].

Twenty individual readings were taken with the crawler being lifted and realigned between each measurement. The Vicon data was taken as the ground truth of the crawlers distance from the edge and was used to evaluate the perceived distance from the edge calculated using the D435i's point cloud.

This process was repeated for multiple different scenarios including altered light levels and different material surface finishes. The altered light levels were carried out to simulate light gradients measured within a typical on-site store which ranged 294 to 1390 lux. To cover this range, measurements were taken at low, medium, and high light levels – 240, 886, and 1708 lux – as well as extreme low light conditions – 2 lux. The surface finish of the plate was then altered to better understand the capabilities of the camera and to explore how it would perform on materials other than matt steel. Paper was used to cover the plate and simulate materials with a higher reflectivity and remove any surface variation. A polished Aluminum plate was also assessed to test the D435i's performance on mirror-like reflective surfaces.

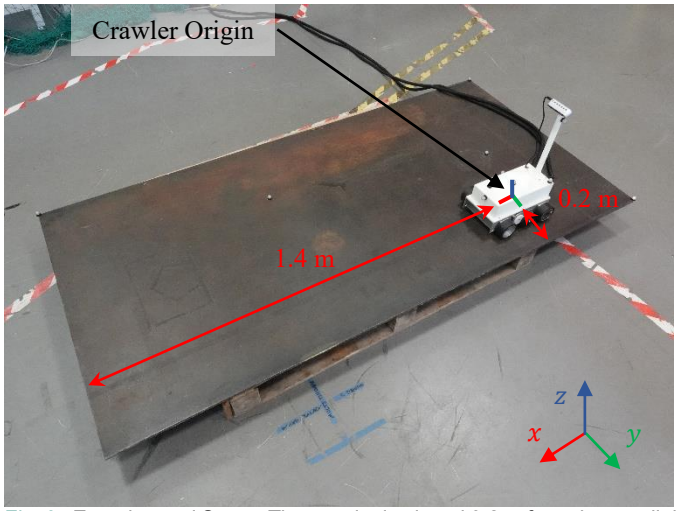

Fig. 3. Experimental Setup. The crawler is placed 0.2 m from the parallel edge and 1.4 m from the perpendicular edge. This is also the starting point for dynamic testing.

Each test configuration is equated by the root mean square error (RMSE) for several parameters including the planar surface consistency of the plate, the estimated distance from the plates edge for all points, and the calculated distance and skew of the crawler relative to the edge. RMSE being a measure of how well estimated/predicted data matches the observed/true data, for the procedure depicted, it acts as a measure of performance between the different configurations [26], [27].

In addition to static testing of the camera, dynamic analysis was conducted by recording the crawler origin (Fig. 3), as it traversed the plate. The Vicon system was utilized to record the true position of the crawler which is compared to the estimated distance from the edge. This was done to highlight any inconsistencies of the differential drive algorithm and to find differences in error between dynamic and static testing. A dynamic measurement also provides a better indication of the ability of the system to replicate the desired path consistently.

III. Edge Detection and Localization Algorithm

A. Data Capture & Manipulation

Point cloud images are used to assess the environment around the crawler. Working with other elements of the system images are captured at a rate of 10 Hz. A disadvantage of point clouds are their large memory occupancy and inherently longer processing time. To counter this the cloud is cropped on two separate occasions to minimize the number of points which do not contribute to the localization of the system, Fig. 4 (a)-(d).

Due to the pitch of the camera the raw point cloud is not aligned with the world frame. 3D rotational matrices are applied to align the point cloud into a processable state [28]. Initially two points from the cloud, one from the plate itself, Fig. 4 (b)(i) and another simulated from the desired final position which is equivalent to the true planar position of the real-world plate, Fig. 4 (b)(ii). The angle between these points is calculated and implemented within the matrices. This is first applied to correct around the y-axis, then repeated around the x-axis, Fig. 4 (b)-(d). The camera origin is also misaligned from the crawler origin so during this process the cloud is translated to account for this.

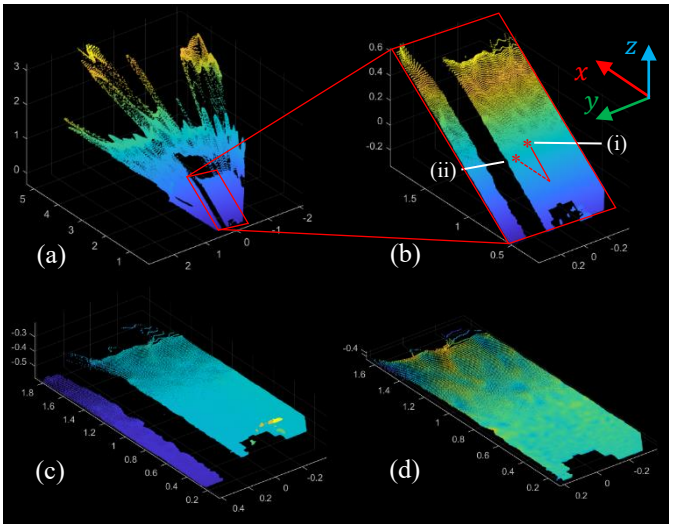

Fig. 4. (a) Raw point cloud image (b) First crop and angle for y-axis rotation (c) Rotated point cloud (d) Second crop resulting in final point cloud.

B. Edge Processing

Upon matching the point cloud to the world frame, it is possible to pull the edge of the plate from the data. An algorithm was developed to extract points along the edge in a raster pattern as described below.

Algorithm Edge Processing
Result: *Distance and relative skew angle from crawler origin to parallel and perpendicular plate edge*

Initialization:
1 Capture point cloud.
2 Crop and reorient cloud to match the crawler reference frame.
Parallel Edge Processing:
3 **For** m = 1:100
4 Take mth segment for processing starting from x = 0.27
For n = 1:10
5 Take nth section of segment starting from y = 0
6 Parse sections applying the following conditions
1) Find maximum y-coordinate
2) Check no points occupy the following section
End For
7 Store individual parallel point for averaging.
End For
8 Split points from step 7 into two equal sections
9 Average 1st and 2nd section to find start and end point of projection line.
10 Create projection line using averaged points from step 9.
11 Find estimated parallel edge from the projection line and calculate *parallel distance* and *skew angle*.
Perpendicular Edge Processing
12 Recall previous distance to perpendicular edge
For m = 1:100
13 Take mth segment for processing starting from y = -0.1
15 Find maximum x-coordinate from x = previous est. ± 0.1.
16 Store individual perpendicular point for averaging.
End For
17 Average 100 perpendicular points taken from step 16.
18 Use averaged points from step 17 to calculate *perpendicular distance*.

Table 3
Parameter values for edge processing.

Variable Name	Value (m)
Parallel Edge Start	0.27
Parallel Edge Segment Width	0.06
Section Width	0.05
Perpendicular Edge Start	-0.1
Perpendicular Edge Segment Width	0.02
Perpendicular Estimate	Previous prediction
Perpendicular Edge Range	0.1

For the application, variables and values given in Table 3 were selected. The parallel edge detection starts at 0.27 m as a shadow is created by the front end of the crawler. 6 mm wide segments are then selected implying over 100 measurements and 600 mm of plate edge is stored for further processing. For each segment a 5 mm section is checked for the highest y-coordinate point, when the following section is empty, this point is saved as shown in Fig. 5 (a).

Due to the position and orientation of the camera it cannot directly see the parallel edge of the plate in-line with the origin of the crawler. The true distance from the crawler to the plate edge must therefore be estimated through projecting the edge, Fig. 5. This is done by splitting the points into two sections by half and creating two points from the average of each section. These two points create a projection line as shown in Fig. 5 (b) The projected edge is at the intersection of this line and the y-axis, as depicted in Fig. 5 (b). This averaging also allows for the calculation of the relative skew angle between the central plane of the crawler along its local x-axis and the edge of the plate. In Fig. 5 (c) an example of the actual point cloud data is displayed with relevant features from Fig. 5 (b) and Fig. 5 (c) highlighted for clarity. This projected edge and skew angle are then used to calculate the crawler's wheel speeds.

A similar edge processing method is applied for the perpendicular edge but instead of running from the central plane of the crawler, Fig. 5 (a), the previous estimate of the perpendicular edge is used as a base with the maximum x-coordinate stored from over a range about the previous estimate ± 0.1 m. The resultant values from the edge processing algorithm are the distances of crawler origin to both parallel and perpendicular edge and the relative skew angle of the crawler in relation to the parallel edge as Fig. 5 (c).

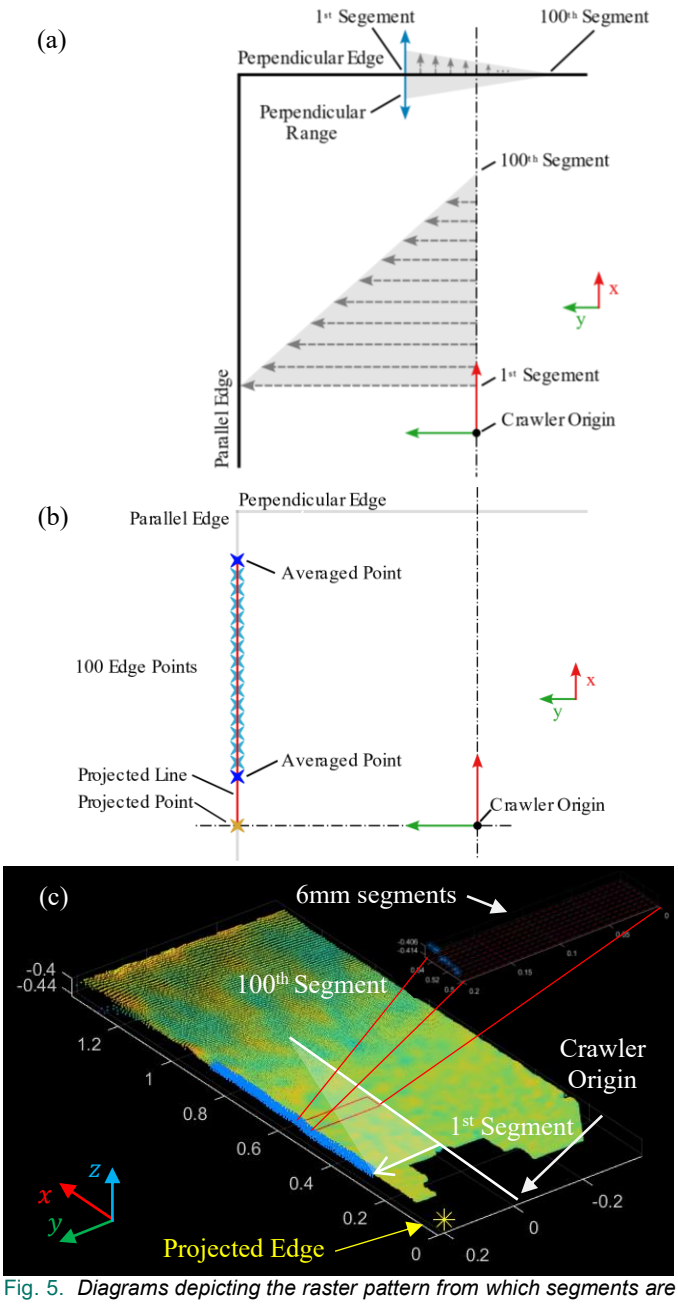

Fig. 5. *Diagrams depicting the raster pattern from which segments are selected for processing. (a) Segments are taken positively in the x-direction and negatively in the y-direction. (b) Details of forming the projection line from two sections of averaged points. (c) Actual point cloud data captured during testing, a cluster of 6 mm segments are also highlighted.*

C. Crawler Locomotion

To position and orient the crawler proportional feedback control (P-control) is utilized to update the differential drive of the crawler. To ensure its safety the algorithm was set to run the crawler 200 mm from the edge of the plate starting 0.2 m from the parallel edge and 1.4 m from the perpendicular edge, a position seen in Fig. 3. A target system is implemented as seen in Fig. 6.

Where:

- T_x and T_y are the target coordinates relative to the plates edge ($T_x = 150\ mm, T_y = 200\ mm$).
- C_x and C_y is the current crawler position ($C_x = 0\ mm, C_y$ is equal to the projected edge).
- T_θ is the target skew of the crawler such that the crawler would be directly approaching the target if $T_\theta = C_\theta$.
- C_θ is the current crawler skew calculated using the averaged parallel edge read by the D435i.

Using a target system based upon the desired angle of the crawler aids in limiting any position related instability. Specifically, it reduces the overshoot that would be expected if making a direct comparison between the target and projected edge, T_y and C_y.

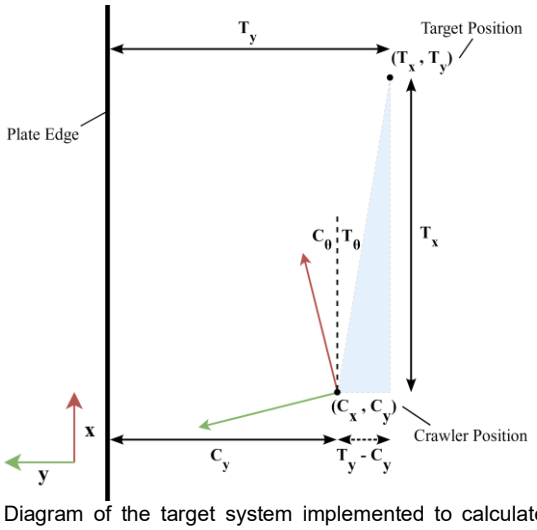

Fig. 6. Diagram of the target system implemented to calculate and update the differential wheel speeds of the crawler.

The target skew is calculated using the four-quadrant inverse tangent shown in equation (1) which is carried forward into the P-control equations (2)-(4).

$$T_\theta = A\,tan2\left(T_y - C_y,\ \ T_x\right) \quad (1)$$

$$\theta_{error} = T_\theta - C_\theta \quad (2)$$

$$v_{lw} = v_s - (K_p \times \theta_{error}) \quad (3)$$

$$v_{rw} = v_s + (K_p \times \theta_{error}) \quad (4)$$

Where:

- θ_{error} is the difference between the crawler's actual skew and the target skew.
- v_{lw} and v_{rw} is the left and right wheel velocities.
- v_s is the set wheel velocity ($v_s = 40\ mm/s$).
- K_P is the proportional gain ($K_p = 15$).

The set wheel velocity of 40 mm/s is the standard velocity of the crawler if running unaltered by the localization algorithm.

IV. Results & Discussion

A. Static Testing

The results for all static testing can be found within Table 4. The first parameter evaluated was the surface deviation associated with measurements taken from the point cloud of a plate which is known to be flat to a degree lesser than the camera resolution. To ensure the camera captures a consistent reading of the plate, a comparison was made between the ground truth height of the camera above the surface, and the z-values of the plate as read by the camera. This was to highlight any early implications of noise between scenarios which could be detrimental to readings, see Fig. 7. The error values indicate that D435i's ability to see and detect the surface of the plate is consistent across all test scenarios. Displaying the camera's competence to see bulk objects within a test environment. Minimal noise between frames also reduces the risk of presenting false artefacts which could have an adverse effect on the edge detection algorithm.

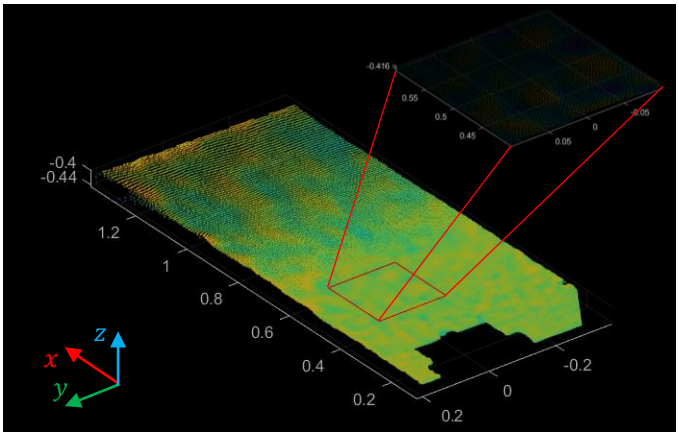

Fig. 7. Point cloud segment used to process the noise associated with the z-axis of the plate.

The second parameter evaluated was the noise linked with the various points extracted from the edge during the segmented raster with respect to the y-axis, Fig. 5 highlighted in blue. This provides a better understanding of the D435i's ability to find the edge of the plate consistently and accurately and identify any test which has the presence of anomalous points.

The noise associated with detecting the edge of the plate is consistent across the tests with a notable increase for the aluminum sample indicating an inability to properly see the true edge. Through closer inspection of the raw point cloud the source is found to be measurements taken from the far edge of the plate ($0.5 < x < 0.8$ m) where the angle of reflection is higher, thus resulting in gaps of data occurring within the point cloud that reduce the number of samples within a given capture.

A similar trend seen for noise associated to the plates edge along the y-axis is apparent in the RMSE for the predicted skew of the crawler. With the aluminum providing the camera's lowest performance for the same reason stated but to an acceptable degree made possible by the averaging of the points. The same cannot be said for the projected edge RMSE on aluminum, rendering the localization system inoperable. Stronger results can be seen for the remaining tests with the lowest performance noted for the extreme low light condition

Table 4
Collection of RMSE data for noise about the z and y axes along with the estimated edge and relative skew between the crawler and the plate edge.

Test Configuration	Z-Noise RMSE (mm)	Y-Noise RMSE (mm)	Estimated Edge RMSE (mm)	Skew RMSE (°)
Steel Very Low Light (2 lux)	0.2	5.5	8.0	0.1
Steel Low light (240 lux)	0.4	4.2	3.7	0.1
Steel Medium light (886 lux)	0.4	5.9	2.5	0.3
Steel High Light (1708 lux)	0.7	4.3	2.8	0.1
Paper Low Light (210 lux)	0.8	5.5	6.5	0.3
Aluminum Low Light (218 lux)	1.1	80.7	202.9	2.9

where the edge is harder to distinguish from the background, and for paper where the higher reflectivity of its surface caused some inconsistencies.

Overall, the RMSE values across the simulated light gradient for the standard steel plate are of a high standard where the edge can be seen reliably, as a result, an accurate projection can be calculated for the crawler's distance to the edge and skew.

B. Dynamic Testing

To properly understand the implications of these RMS errors on practical results a dynamic test was run under low light conditions. The same static testing algorithm was implemented with proportional control as described in Section III.C which is set to maintain the crawler 200 mm from the plate edge. The crawler's true position was recorded during this time using the Vicon system and both the target and true parameters were then compared against the estimated distance from the edge across 1 m of travel.

Taking the true and estimated distance, the mean error between the two readings was 3.9 mm with a standard deviation of ± 2.5 mm. The RMSE related to the data collected over this test for edge estimation was 4.6 mm and for skew estimation was 0.49 ° which correlates with the performance of the static testing, 3.7 mm and 0.10 °, respectively.

The true position of the crawler varies due to it constantly correcting its trajectory, resulting in average distance from the edge of 194.3 mm and therefore a mean error of 5.7 mm with a standard deviation of ± 5.0 mm. The RMSE associated with the target vs estimated distance from the plate edge is 4.6 mm.

A systematic error was present which is made apparent by the difference between the estimated edge error and the target position error. This can be attributed to a number of factors such as initial camera orientation, structural vibrations, wheel slip, and inconsistencies between the differential drive motor velocities. However, even with the error present, the resulting positional accuracy is still within that expected from an NDE inspector carrying out the procedure.

An example of the stored edge during a full traversal of the steel plate is shown in Fig. 8, constructed from data taken in low light conditions (240 lux).

The figure is constructed from points taken at every instance a point cloud was processed. The crawler position indicated by the points in black are taken by the Vicon system while the blue points represent the projected edge estimated for the given location. The consistent trajectory of the crawler indicates the promise of the system with gradual adjustments being made to correct any drift that occurred while running. The estimated edge is also consistent during this time with only four points occurring outside ± 2 standard deviations.

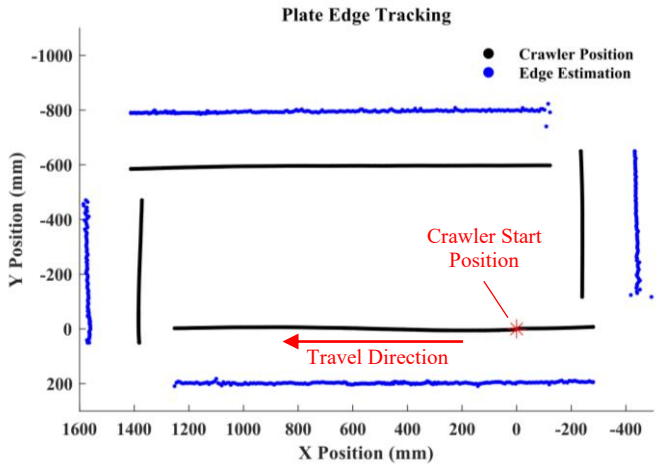

Fig. 8. Plot of crawler position and estimated edge during a full, clockwise traversal of the steel plate.

V. Conclusion

Given the application of the receipt inspection of steel plate a novel method of robotic localization has been presented which utilizes a 4-wheel differential drive crawler with an onboard Intel RealSense D435i camera. This particular inspection can be laborious, and time consuming for the inspector and can profit from the addition of robotic crawler support.

A method for crawler localization is detailed involving the capture of point cloud images followed by post-processing of the data to detect the edges of the plate, which in turn are used to determine the orientation of the crawler.

A major benefit of such a system is the lack of external factors required to track and position the crawler, relying solely on generic features of the inspection material to navigate across the plate. The receipt inspection of steel plate also exhibits characteristics which imply the localization system developed here can be applied to a wide range of scenarios. The surface is planar and semi-structured while also showing self-similarity in a feature-sparse environment.

Experiments were conducted to better understand the capabilities of the D435i camera which were validated through the Vicon motion capture system. This included assessing the edge detection algorithm on different surface types and importantly, simulated the various light levels present within the area of inspection. During static testing, for a standard steel plate located in a 240 lux environment, the distance and relative skew between the crawler and plate edge was calculated with a root mean square error of 3.7 mm and 0.10 °. This translates to a physical positional accuracy measured during dynamic testing of 5.7 ± 5.0 mm with an estimated edge RMSE of 4.6 mm and

estimated skew RMSE of 0.49 °. Referring to the accuracy attained by systems with prior knowledge of the inspection component, examples were shown to be capable of positioning the crawler within 5-10 mm of the desired position, the accuracy attained using the method described in this paper is comparable and advantageous considering that minimal assumptions are required to process the data.

To reduce the systematic error and increase the general accuracy of the system, a redesign of the crawler platform is planned which would reduce mechanical factors contributing to the error with a more robust locomotion base and optimized camera placement and support. The system is also to be tested in other semi-structured self-similar environments to explore its performance in a range of settings.

REFERENCES

[1] G. Dobie, R. Summan, S. G. Pierce, W. Galbraith, and G. Hayward, "A Noncontact Ultrasonic Platform for Structural Inspection," *IEEE Sens. J.*, vol. 11, no. 10, pp. 2458–2468, Oct. 2011, doi: 10.1109/JSEN.2011.2138131.

[2] R. Bogue, "The role of robotics in non-destructive testing," *Ind. Robot*, vol. 37, no. 5, pp. 421–426, 2010, doi: 10.1108/01439911011063236.

[3] D. Lattanzi and G. Miller, "Review of Robotic Infrastructure Inspection Systems," *J. Infrastruct. Syst.*, vol. 23, no. 3, p. 04017004, Sep. 2017, doi: 10.1061/(ASCE)IS.1943-555X.0000353.

[4] "Scorpion 2 Ultrasonic Tank Shell Inspection | UT Thickness Readings." https://www.eddyfi.com/en/product/scorpion-2 (accessed Aug. 23, 2022).

[5] "Nuclear Solutions-Robotic Online Storage Tank Floor Inspection." https://www.diakont.com/nuclear_solutions/170/robotic-online-storage-tank-floor-inspection.html (accessed Aug. 23, 2022).

[6] "NAVIC," *JIREH*. //www.jireh.com/navic/ (accessed Aug. 23, 2022).

[7] "Motorised TOFD & Phased Array Weld Scanner | Phoenix SAW Bug," *Phoenix ISL*. https://www.phoenixisl.com/product/saw-bug/ (accessed Aug. 23, 2022).

[8] viktor, "FAST UT – Inspection Robotics." https://inspection-robotics.com/fast-ut/ (accessed Aug. 23, 2022).

[9] S. Thrun, "Probabilistic robotics," *Commun. ACM*, vol. 45, no. 3, pp. 52–57, Mar. 2002, doi: 10.1145/504729.504754.

[10] K. Krinkin, A. Filatov, A. Filatov, A. Huletski, and D. Kartashov, "Evaluation of Modern Laser Based Indoor SLAM Algorithms," presented at the Proceedings of the XXth Conference of Open Innovations Association FRUCT, May 2018, vol. 426, pp. 101–106. doi: 10.23919/FRUCT.2018.8468263.

[11] C. Ulas and H. Temeltas, "A Fast and Robust Feature-Based Scan-Matching Method in 3D SLAM and the Effect of Sampling Strategies," *Int. J. Adv. Robot. Syst.*, vol. 10, no. 11, Nov. 2013, doi: 10.5772/56964.

[12] P. Tripicchio, M. Unetti, N. Giordani, C. Avizzano, and M. Satler, "A lightweight SLAM algorithm for indoor autonomous navigation," Jan. 2014.

[13] M. Skoczeń *et al.*, "Obstacle Detection System for Agricultural Mobile Robot Application Using RGB-D Cameras," *Sensors*, vol. 21, no. 16, p. 5292, 2021, doi: 10.3390/s21165292.

[14] A. McGregor, G. Dobie, N. R. Pearson, C. N. MacLeod, and A. Gachagan, "Determining Position and Orientation of a 3-Wheel Robot on a Pipe Using an Accelerometer," *IEEE Sens. J.*, vol. 20, no. 9, pp. 5061–5071, May 2020, doi: 10.1109/JSEN.2020.2964619.

[15] D. Zhang, J. Cao, G. Dobie, and C. MacLeod, "A Framework of Using Customized LIDAR to Localize Robot for Nuclear Reactor Inspections," *IEEE Sens. J.*, vol. 22, no. 6, pp. 5352–5359, Mar. 2022, doi: 10.1109/JSEN.2021.3083478.

[16] R. Summan *et al.*, "Spatial calibration of large volume photogrammetry based metrology systems," *Measurement*, vol. 68, pp. 189–200, May 2015, doi: 10.1016/j.measurement.2015.02.054.

[17] "Laser Tracker Systems," *Hexagon Manufacturing Intelligence*. https://www.hexagonmi.com/en-GB/products/laser-tracker-systems (accessed Sep. 09, 2022).

[18] M. Tabatabaeipour, O. Trushkevych, G. Dobie, R. S. Edwards, C. Macleod, and S. G. Pierce, "Guided Wave Based-Occupancy Grid Robotic Mapping," in *European Workshop on Structural Health Monitoring*, Cham, 2021, pp. 267–275. doi: 10.1007/978-3-030-64908-1_25.

[19] R. Feng, R. T. Zhang, S. L. Li, G. H. Kong, and X. D. Zhu, "Study on Forming Mechanism of Lamination Defect of AH36 Shipbuilding Plate Steel," *Adv. Mater. Res.*, vol. 562–564, pp. 106–110, 2012, doi: 10.4028/www.scientific.net/AMR.562-564.106.

[20] Y. Wang, H. Chen, S. Zhang, and W. Lu, "Automated camera-exposure control for robust localization in varying illumination environments," *Auton. Robots*, vol. 46, no. 4, pp. 515–534, Apr. 2022, doi: 10.1007/s10514-022-10036-x.

[21] D. Zhang *et al.*, "Remote inspection of wind turbine blades using UAV with photogrammetry payload," in *56th Annual British Conference of Non-Destructive Testing - NDT 2017*, GBR, Sep. 2017. Accessed: Dec. 13, 2022. [Online]. Available: https://strathprints.strath.ac.uk/63321/

[22] "Depth Camera D435," *Intel® RealSense™ Depth and Tracking Cameras*. https://www.intelrealsense.com/depth-camera-d435/ (accessed Aug. 23, 2022).

[23] M. S. Ahn, H. Chae, D. Noh, H. Nam, and D. Hong, "Analysis and Noise Modeling of the Intel RealSense D435 for Mobile Robots," in *2019 16th International Conference on Ubiquitous Robots (UR)*, Jun. 2019, pp. 707–711. doi: 10.1109/URAI.2019.8768489.

[24] I. El Bouazzaoui, S. Rodriguez, B. Vincke, and A. El Ouardi, "Indoor visual SLAM dataset with various acquisition modalities," *Data Brief*, vol. 39, p. 107496, Dec. 2021, doi: 10.1016/j.dib.2021.107496.

[25] E. Tsykunov, V. Ilin, S. Perminov, A. Fedoseev, and E. Zainulina, "Coupling of localization and depth data for mapping using Intel RealSense T265 and D435i cameras." arXiv, Apr. 01, 2020. doi: 10.48550/arXiv.2004.00269.

[26] K. Tiwari and N. Young Chong, "8 - Informative Path Planning (IPP): Informative area coverage," in *Multi-robot Exploration for Environmental Monitoring*, K. Tiwari and N. Young Chong, Eds. Academic Press, 2020, pp. 85–99. doi: 10.1016/B978-0-12-817607-8.00021-6.

[27] C. N. MacLeod, R. Summan, G. Dobie, and S. G. Pierce, "Quantifying and Improving Laser Range Data When Scanning Industrial Materials," *IEEE Sens. J.*, vol. 16, no. 22, pp. 7999–8009, Nov. 2016, doi: 10.1109/JSEN.2016.2601822.

[28] P. Corke, "Representing Position and Orientation," in *Robotics, Vision and Control: Fundamental Algorithms In MATLAB® Second, Completely Revised, Extended And Updated Edition*, P. Corke, Ed. Cham: Springer International Publishing, 2017, pp. 17–62. doi: 10.1007/978-3-319-54413-7_2.